

Journal of Materials Chemistry A

Accepted Manuscript



This is an *Accepted Manuscript*, which has been through the Royal Society of Chemistry peer review process and has been accepted for publication.

Accepted Manuscripts are published online shortly after acceptance, before technical editing, formatting and proof reading. Using this free service, authors can make their results available to the community, in citable form, before we publish the edited article. We will replace this *Accepted Manuscript* with the edited and formatted *Advance Article* as soon as it is available.

You can find more information about *Accepted Manuscripts* in the [Information for Authors](#).

Please note that technical editing may introduce minor changes to the text and/or graphics, which may alter content. The journal's standard [Terms & Conditions](#) and the [Ethical guidelines](#) still apply. In no event shall the Royal Society of Chemistry be held responsible for any errors or omissions in this *Accepted Manuscript* or any consequences arising from the use of any information it contains.

Cite this: DOI: 10.1039/c0xx00000x

PAPER

www.rsc.org/xxxxxx

Microscopy investigations of the microstructure change and thermal response of the cobalt-based nanoparticles confined inside carbon nanotubes medium

Walid Baaziz,^{*a} Ileana Florea,^{b,c} Simona Moldovan,^b Vasiliki Papaefthimiou,^a Spiridon Zafeiratos,^a Sylvie Begin-Colin,^b Dominique Begin,^a Ovidiu Ersen,^{*b} and Cuong Pham-Huu^a

Received (in XXX, XXX) Xth XXXXXXXXX 20XX, Accepted Xth XXXXXXXXX 20XX

DOI: 10.1039/b000000x

Faceted cobalt-cobalt oxide based nanoparticles (NPs) with high density and narrow size distribution (50 ± 5 nm) were selectively casted inside the channels of multi-walled carbon nanotubes (CNTs) through the controlled thermal decomposition of cobalt stearate in the presence of oleic acid as surfactant. The total loading of the NPs is ca. 60 wt % due to the confinement effect of CNTs, which play the role of "nanoreactors" for the cobalt complex filling and its further decomposition. The casted Co-based NPs are consisted with a Co-CoO core-shell structure with a relatively high contribution of metallic phase thanks to the confinement effect which prevents excessive oxidation. The Co-CoO NPs were transformed into highly porous cobalt aggregates constituted by small cobalt clusters (5 nm) after reduction with a high effective surface area. These cobalt clusters display an extremely high resistance towards oxidation thanks to the confined medium. The evolution of the Co-based NPs microstructure of the as-synthesized and the reduced composites, as a function of temperature, was evaluated by in situ heating the systems inside the TEM. On the as-synthesized sample with a mixture of Co and CoO the heating process leads to a rapid shape modification and coalescence of the NPs at a temperature of 400°C along with the formation of a cobalt carbide interface. On the contrary, the reduced sample displays a much higher sintering resistance upon annealing under the same conditions as cobalt NPs with a mean diameter of 10 nm are still present at annealing temperature up to 800°C. The work reported here underlines the benefit of the confinement effect to improve the oxidative and sintering resistance of casted metal NPs and also in the synthesis of new porous structure containing small metal NPs which could be of high interest for catalytic and magnetic applications.

1. Introduction

In recent years, magnetic nanoparticles (NPs) have received an ever growing attention and several current issues in NPs research focus on the development of new synthetic strategies to control their structural and magnetic properties. Such nanostructures were found to exhibit physical and chemical properties significantly different from the bulk materials, and can be promising for several nanotechnology applications including heterogeneous catalysis [1-5] and biomedicine [6-12]. However, unsupported or "naked" NPs tend to aggregate together in order to reduce their surface free energy and their nanoscopic size renders them more sensitive towards oxidation or corrosion upon air exposure, i.e. pyrophoric character or surface oxidation process leading to the alteration of the pristine NPs properties,

which severely limits their applicability. Therefore, major efforts have lately been devoted to synthesize magnetic NPs sufficiently protected against such degradations by encasing them into inert chemical components such as polymers and carbon nanostructures [13-16].

Since the first report on the unique electronic and mechanical properties of carbon nanotubes (CNTs) in 1991 [17], these materials have generated broad and interdisciplinary scientific interest. The methods of CNTs synthesis, opening, filling, as well as their wetting and filling properties have been largely explored [18-22], but the possibility of using their inner channels as nano-sized reactors still remains an exciting challenge regarding the potential fields of application. In fact, the combination of these two classes of materials (CNTs and NPs) significantly modifies their intrinsic properties, leading to the development of new hybrid materials. In this context, the development of nanopeapod-

like structures for specific applications is a hot research topic, not only from a fundamental point of view but also for potential industrial interest use [23-30].

The magnetic NPs in association with such a 1D spatial arrangements as the CNTs are strongly susceptible to develop interesting anisotropic and collective properties [31-35], which are of extreme interest for applications in the domains of magnetism, catalysis and nanotechnology. In previous work, we have synthesized $\text{Fe}_{3-x}\text{O}_4$ NPs selectively deposited inside or on the outer surface of CNTs and we observed that the NPs display magnetocrystalline anisotropy higher than the unsupported ones, due to the dipolar interactions that are more important in this arrangement [36]. Recently, Fu *et al.* have reported the synthesis of spherical Co_3O_4 NPs in multi-walled CNTs for the electrical transport in electronic devices using the supercritical-solution method [37]. Also, Trépier *et al.* have synthesized cobalt NPs in CNTs by incipient wetness impregnation of cobalt nitrate solution. The as-prepared nanomaterial with 30 wt % of cobalt loading was further tested as catalyst for the Fisher-Tropsch reaction with 86 % of CO conversion [38].

The control of the filling process within the tubes channel is mandatory for a good optimization of the properties of such hybrid materials. The researchers currently employ techniques such as the incipient wetness impregnation by capillarity (with NPs or metal salt in solution) [23, 38, 39], the sublimation of metal precursors in CNTs cavity [40, 41] or by producing CNTs inside anodic membranes followed by the filling of resulting template with NPs solution following by a thermal treatment steps and subsequent membrane dissolution [35, 42]. The main drawback while using such synthesis methods relates to the low filling rates and a selectivity less than 50 %, which implies significant lost of precursor and/or NPs and as a consequence the production costs are considerably high (especially in the case of anodized alumina membrane). In addition, the microstructural shape of the NPs is not well controlled which could hinder their downstream application.

The morphological modification upon confining has been reported elsewhere [43]. The aim of this work is to report on the benefit of confinement medium on the enhancement of both oxidative and sintering resistance of cobalt-based NPs casted within multi-walled CNTs, with a total filling of 60 wt%, which are synthesized by using a solvothermal method. We have also investigate the pseudomorphism transformation of the mixed cobalt composite (Co-CoO) during the reduction step into a metallic cobalt clusters with a highly porous structure along with high oxidative resistance. Finally, a detail investigation on the influence of a pre-reduction step on the sintering behavior of the confined cobalt NPs will be carried out by in situ heating process and a mechanism of sintering will be discussed. These peculiar physical properties are obtained by combining several characterization techniques including transmission electron microscopy (TEM)-based techniques: HR-TEM and STEM-HAADF imaging and tomography, EEL spectroscopy, with the X-ray Photoelectron Spectroscopy (XPS), X-ray diffraction (XRD) and magnetic measurements. Such a multi-scale and multi-selective approach provides valuable details concerning the microstructure and the crystallographic orientation within the cobalt-based NPs in confinement medium. The reactivity and

structural change of the confined NPs will be also investigated through in situ reduction inside the microscope. The results indicate that by such approach one is able to synthesize new class of porous metal hybrid with an extremely small particle size for numerous potential applications.

2. Experimental

2.1. Carbon nanotubes support.

Hollow vapor-grown multi-walled CNTs (Pyrograf Products) were used as starting materials for the filling with NPs. The CNTs present a straight and open-ended channel (excluded some exceptions) with an average inner diameter between 40 and 60 nm. Before filling, the CNTs were annealed under argon flow at 900 °C for 2 h in order to remove the oxygenated functional groups from their surface which could lead to a side-adsorption reaction during the filling process.

2.2. Co-CoO@CNTs.

The synthesis method consists in the thermal decomposition of cobalt stearate in the presence of oleic acid as surfactant and the adequately pre-treated CNTs. More precisely, 50 mg of CNTs previously defunctionalized under argon were suspended in 20 mL of octadecene (Alfa Aesar, 90%) under ultrasonication for 10 minutes. After adding 1.389 g (2.2 mmol) of cobalt stearate (Strem Chemicals, 9-10% Co) and 1.4 mL (4.4 mmol) of oleic acid (Alfa Aesar, 99%), the reaction medium was heated up to 120 °C under stirring overnight in order to dissolve the reactants and to eliminate traces of water or dissolved impurities. The system was heated up to reflux (318 °C) under argon atmosphere with a heating rate of 5 °C min⁻¹. The reaction was allowed to stand for 2 hours at this temperature.

After cooling at room temperature, the NPs and CNTs were first precipitated by adding to the suspension an excess of acetone and then centrifuged (8000 rpm, 10 min). The resulting black precipitate was then washed 3 times by adding a mixture of hexane and acetone (50:50), then centrifuged (8000 rpm, 10 min) and filtered to separate the NPs synthesized outside the CNTs.

In order to identify the confinement effect on the synthesized cobalt-based NPs, similar preparation method was performed but by replacing the CNTs with another support consisting in of few layer graphene (FLG) (200 mg), which has been prepared by mechanical ablation of graphitic materials (pencil lead) [44]. The same purification approach was used.

2.3. Metallic Co@CNTs.

The reduction of the core-shell Co-CoO-based@CNT was carried out in a tubular quartz oven under hydrogen flow at 400 °C (heating rate of 2 °C/min) during 2 hours. The resulted material was cooled down to room temperature under H₂. To avoid any excessive oxidation of the sample, a passivation treatment using a gas mixture containing 1% of oxygen in helium for 30 minutes was applied to the sample prior to its removal from the oven.

2.4. Characterization Techniques.

The classical TEM observations, HAADF-STEM EELS analysis and HAADF-STEM tomographic experiments have been performed using a JEOL 2100F TEM/STEM electron microscope equipped with a Cs probe corrector, GIF Tridiem filter and a

tomographic set-up. The traditional and high-resolution images were acquired using both the HAADF-STEM and BF modes. The STEM EELS analysis and the corresponding HAADF images of the selected areas were recorded using a 0.2 nm electron probe and an energy dispersion of 0.3 eV/channel, with an acquisition time of 3 sec/pixel for each EEL spectrum.

For the tomography experiments, the HAADF-STEM tilt series were acquired using the ADF detector by tilting the specimen in the angular range of $\pm 70^\circ$ using an increment of 2.5° in the equal mode, giving thus a total number of images equal to 57 images in the series. The relatively large inner radius chosen for the ADF detector, 40 mrad, allowed us to consider that the intensity in the corresponding images scales with the mean atomic number. Finally, the gain of the ADF detector was chosen such that any saturation effect in the HAADF images during the series acquisition was prevented. The images of the tilt series were spatially aligned using in a first step cross correlation functions applied to the consecutive images, followed by a fine alignment procedure in which the NPs were considered as fiducial markers. Both procedures used for the alignment are implemented in the IMOD software [45]. For the volume calculation, we have used iterative methods as they are more accurate than the one-step ones, providing high quality reconstruction volumes even from series with rather limited number of projections. The algebraic reconstruction techniques (ART) [46] implemented in the TomoJ macro [47] working in the ImageJ software [48] were used to obtain the reconstructed volumes of the analyzed sample presented in this paper. Finally, the volumes visualization and the analysis were carried out using the displaying capabilities and the isosurface rendering method in the Slicer software [49].

The X-ray photoelectron spectroscopy (XPS) measurements were carried out in an ultrahigh vacuum (UHV) setup equipped with a VSW ClassWA hemispherical electron analyzer (150 mm radius) with a multi-channeltron detector. A monochromated AlK α X-ray source (1486.6 eV; anode operating at 240 W) was used as incident radiation. The base pressure in the measurement chamber was $\sim 1 \times 10^{-9}$ mbar. XP spectra were recorded in the fixed transmission mode using pass energy of 20 eV resulting in an overall energy resolution better than 0.4 eV. The binding energies were calibrated based on the graphite C 1s peak at 284.5 eV. The thermal treatment of the CNTs was carried out in the preparation chamber of the apparatus for 60 min at each temperature. After each treatment, the samples were transferred under UHV conditions to the analysis chamber. Prior to individual elemental scans, a survey scan was taken for all the samples to detect all of the elements present. The CASA XPS program with a Gaussian-Lorentzian mix function and Shirley background subtraction was employed to deconvolute the XP spectra. The % oxygen content was calculated by O 1s and C 1s core level peaks, properly normalized to the photoemission cross section and assuming a homogeneous distribution arrangement model.

The specific surface area measurements were performed with a Micromeritics Tristar 3000 porosimeter using N $_2$ as adsorbent. The surface area of the sample was calculated from the nitrogen isotherm using the BET method. Before measurements, the sample was outgassed at 250°C for 2h in order to remove the

moisture from its surface.

The powder X-ray diffraction (XRD) experiments were carried out with a Bruker D8 diffractometer. The XRD pattern was recorded in the $30\text{--}65^\circ$ (2θ) range with a scan step of 0.03. Profile matching refinement was performed through the Fullprof program [50] using the modified Thompson Cox Hasting (TCH) pseudo-Voigt profile function [51].

Magnetization measurements were carried out using a Quantum Design MPMS SQUID-VSM magnetometer. Magnetization curves as a function of the applied magnetic field have been measured at 400 and 5 K by sweeping the magnetic field from +5 T to -5 T, and then from -5 T to +5 T.

3. Results and discussion

3.1. Carbon nanotubes support.

Low and high-resolution TEM micrographs of the pristine CNTs (Fig. 1) show that the tubes are relatively straight with both tips opened, except from a few cases (as indicated by arrows). The average length of the tubes corresponds to few tenths of micrometers, the average outer diameter is of about 110 ± 30 nm, the wall thickness of about 15 nm, the inner diameter ranges between 50 and 100 nm, and the specific surface area before filling was around $10 \text{ m}^2/\text{g}$ according to the BET measurement. It is expected that both straightness and large inner diameter of CNTs will have a strong impact on the deposition process of the cobalt-based NPs inside the channels. Indeed, it was reported that CNTs with inner diameters below 30 nm could not be effectively filled by capillarity with solution containing a metal salt precursor [52].

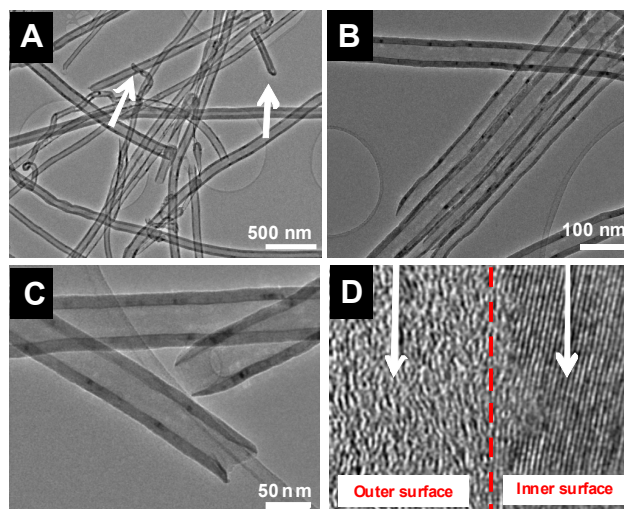


Fig. 1 (A-C) TEM micrographs of the pristine multi-walled carbon nanotubes with open ends. In image (A) the white arrows indicate the presence of few closed ends. (D) High-resolution TEM micrograph showing the presence of an amorphous layer at the outer surface of the CNT.

Also, Figure 1D shows that the outer surface of the CNTs is covered by an amorphous carbon layer, while the inner channel is well structured by the graphitic planes, which could most probably facilitate the interaction with the NPs during the filling process.

In order to explore the different species present on the pristine

CNTs, further analyses by X-ray photoelectron spectroscopy (XPS) was carried out [36, 43]. The XPS survey spectrum of the pristine CNTs (Fig. S1 in Supplementary Information) revealed the existence of oxygenated species on their surface. The atomic concentration of these species was found to be ca. 4.9 %. Deconvolution of the XPS C 1s spectra revealed that the pristine CNTs exhibit components corresponding to single and double carbon-carbon bonds at 284.5 eV and to oxygen-containing moieties C-O (C-O-C, C-O-H), C=O and O-C=O at binding energies between 286.5 eV and 290 eV. Analysis of the corresponding O 1s peak confirmed the presence of C=O and C-O groups resulting from the CNTs synthesis procedure [43]. Such oxygenated functions at the CNTs surface can be considered as anchorage and/or nucleation sites for the NPs growth, which can potentially decrease the filling selectivity [53, 54].

As mentioned previously in the Experimental Section, the CNTs used for this study were pre-treated at 900°C for 2 h under argon, a treatment that is considered efficient enough for the removal of the oxygen functional groups from the tube's surface [55, 56]. The evolution of oxygen during the pre-treatment of CNTs was studied by XPS. As it can be observed in the inset of Figure S1, already at 650 °C a negligible amount of oxygen (ca. oxygen atomic concentration: 0.5 %) was detected on the CNTs surface, confirming the elimination of the oxygenated species by the annealing procedure.

3.2. Co-based NPs @CNT.

3.2.1. Microstructural Investigations.

At first, information concerning the distribution and the microstructure of the as-synthesized Co-based@CNTs were obtained from TEM analysis (Fig. 2). The micrographs clearly indicate that the NPs are homogeneously casted within the CNTs and the presence of several Co-based peapod-like structures as a function of the CNTs channel diameter, i.e. one row of NPs filling the CNTs with an inner diameter of about 50 nm and two rows of NPs filling the CNTs with inner diameter of ca. 100 nm. The TGA curve indicates that the NPs loading is about $60 \pm 5\%$ (Fig. S2A).

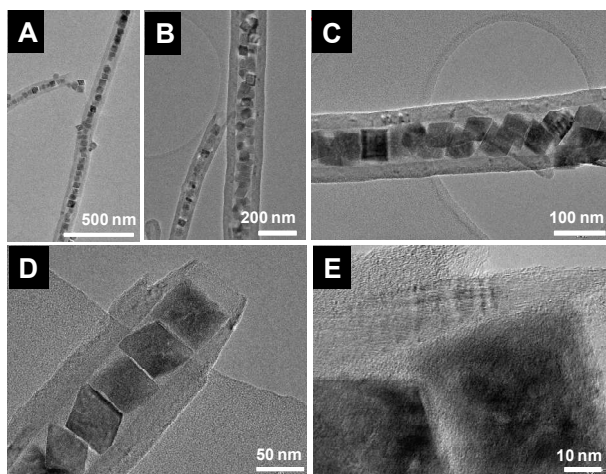


Fig. 2 (A-C) Representative TEM images of Co-based@CNTs structures showing the filling density as a function of the CNTs diameter. (D) Medium TEM micrograph showing the densely packing of the cobalt NPs within the CNT channel. (E) High-resolution TEM micrograph of the cobalt-carbon interface with a smooth interface.

The synthesized Co-based NPs were found to display a faceted shape with a quite narrow size distribution of 50 ± 5 nm (Fig. S2B), which may be associated to the presence of oleic acid that plays the role of the organic surfactant for controlling the nucleation-growth mechanism during the synthesis [57, 58]. One remarks as well the presence of few Co-based NPs on the outer surface of the CNTs (Fig. 2A), which can be easily removed by a repeated washing and magnetic separation. In fact, after removing the oxygenated functions by annealing, the adsorption of NPs on the outer surface of the CNT can be correlated with the structural defects or with the weak intermolecular interactions such as π - π stacking, hydrophobic or electrostatic attractions [59]. In our case, TEM analysis also indicates the extremely high filling selectivity of the CNT channel by the synthesized NPs, which can be attributed to the large inner diameter of the CNTs, as well as to the synthesis conditions with the solution filling-up the tube channel in a continuous way. Indeed, it has been previously reported that CNTs could be easily filled with NPs once the solution with the metal salt precursor was drained in tubes, by capillary forces [52]. The filling rate reported here highlights the advantage of the solvothermal synthesis method to cast metal and/or oxide NPs inside the CNT channel. The high diffusion inside the tube channel is confirmed by TEM showing close end CNTs filled with NPs (Fig. S3). To explain this high filling yield, the following hypothesis can be advanced: the capillarity forces driving the liquid phase inside the CNT's channel were sufficiently high to provide a continuous supply for the cobalt species to grow the cobalt-based particle. Such conditions together with the important cobalt supply induce the formation of a dense cobalt-based network inside the CNT's channel.

It is worth observing that the cobalt-based NPs exhibit a peculiar shape, i.e. octahedral or cube-like structures with sharp facets, as compared with the cobalt-based NPs synthesized in the same conditions but without confinement (see paragraph 3.5 below). In general, the confinement effect only influences the redox behaviour or the catalytic activity of the casted materials as reported by Bao *et al.* [60] and by Nhut *et al.* [61], but has not been reported to influence the shape and the nanostructure of the casted material as observed in the present case.

The crystalline structure of the Co-based NPs was further investigated by X-ray diffraction (XRD). The XRD pattern, in the 30 - 70° (2θ) range, displays the characteristic diffraction peaks of Co and CoO phases (Fig. 3A). An adequate Rietveld refinement, using the Fullprof program, was obtained by considering the presence of these two crystalline phases: Co (JCPDS file n°015-0806) and CoO (JCPDS file n°43-1004). Otherwise, the NPs synthesized without the presence of CNTs were found to display single CoO crystalline structure, certainly due to the excessive oxidation by exposure to the air during the recovery and storage procedures (XRD pattern was added for comparison, Fig. 3B). By contrast, the presence of a relatively large amount of metallic cobalt inside the casted sample indicates that the NPs were sufficiently covered against oxidation due to the presence of the surrounding CNTs acting as "protector" [24].

Electron Energy Loss Spectroscopy (EELS) analyses were carried out on the casted and anchored NPs, to obtain information on their chemical compositions and the Co and O distribution in the NPs volume. In the case of the casted NPs, the Co:O atomic

ratio deduced from the EELS spectra recorded on a line crossing three neighbour NPs, confirms their low oxidation degree (Fig. 4A).

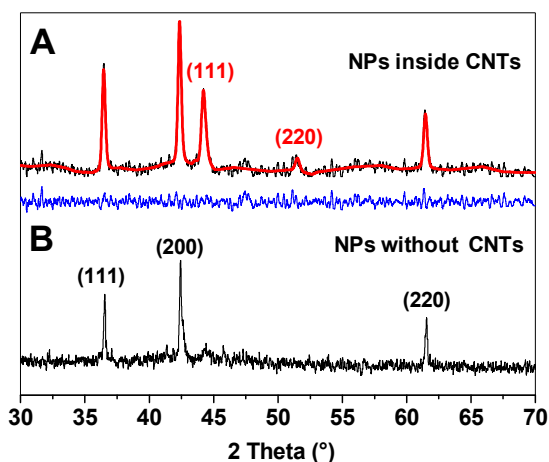


Fig. 3 (A) Experimental (black) and refined (red) XRD patterns of cobalt-based NPs@CNTs after synthesis, showing the presence of Co and CoO crystalline phases. Difference between experimental and refined XRD patterns (blue line). (B) XRD pattern of NPs synthesized without CNTs under the same conditions, showing the presence of only the CoO phase.

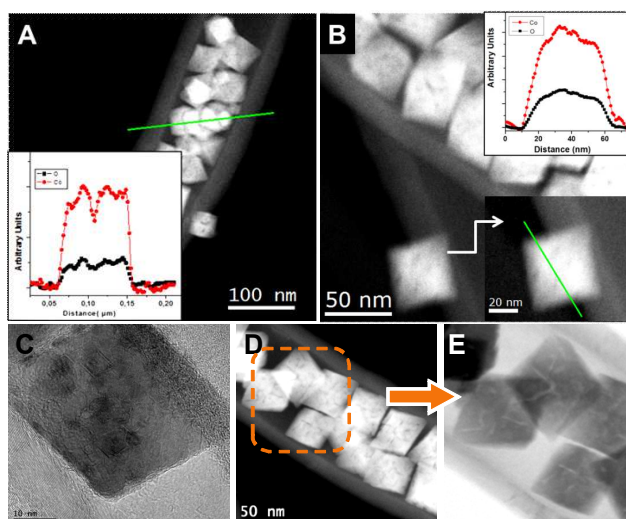


Fig. 4 (A-B) EELS-STEM analyses of the cobalt-based particles located inside and outside the CNTs channel showing the relatively low oxygen content inside the particle. The oxygen content in the EELS line scan represents about 1/5 of the cobalt one. This oxygen can come from surface oxidation of the Co NPs during air exposure. (C) High-resolution TEM micrograph of the interface between the cobalt NP and the inner wall of the host carbon nanotube. (D-E) HAADF-STEM and BF-STEM micrographs suggesting the octahedral morphology of the confined Co NPs inside the CNT channel. The pseudo-fractures can be identified from the 2D HAADF-STEM and STEM-BF micrographs, respectively.

In addition, the evolution of the atoms changes across the particles, suggesting the presence of a non-homogeneous structure from a chemical point of view. On the contrary, the EEL spectra of the NP localized on the outer surface of CNT (Fig. 4B) was found to be more uniform, suggesting the presence of a unique crystalline phase homogeneously distributed on the entire volume of the NP with a higher Co:O atomic ratio. These results are in agreement with those obtained from the XRD analyses,

demonstrating that the CNTs act as nano-shields to prevent the casted NPs against excessive oxidation.

In order to get deeper understandings regarding the influence of the confinement effect on the oxidative resistance of the Co NPs a Co-based NPs supported on few-layer graphene (FLG) synthesized by a mechanical exfoliation of graphitic raw materials [44] with no confinement was synthesized and analyzed. The EELS analyses performed on different areas (Fig. S4) of the cobalt deposited on FLG sample revealed the presence of both Co and oxygen from CoO, for both large NPs and small clusters and no trace of cobalt metal was observed. Such results confirm the high efficiency of the confinement effect provided by the CNTs to enhance the oxidative resistance of the confined metal NPs.

In addition, the TEM analysis clearly indicates that in the absence of a confinement effect, the NPs morphology varies dramatically while the regular octahedral shape which was present in the Co@CNT is no longer observed. Indeed, two types of populations with irregular morphologies and sizes (Fig. 5 and Fig. S5) consisted with star-shape aggregates were observed in the cobalt-decorated on the FLG surface.

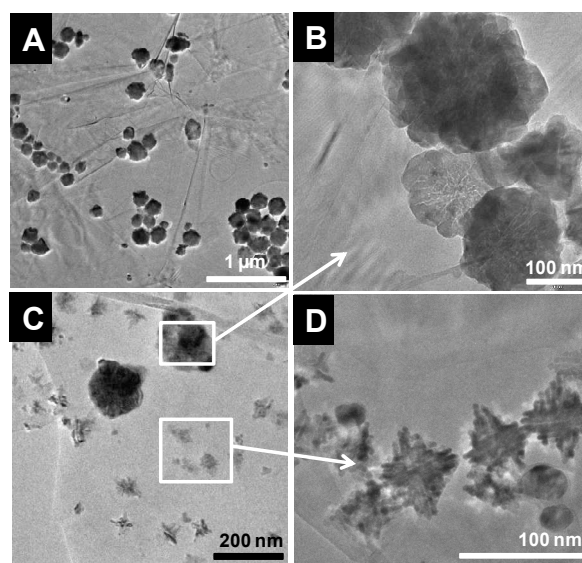


Fig. 5 Representative TEM images of Co-based NPs deposited on FLG surface using the same experimental conditions and showing completely irregular morphologies and size of the NPs.

The growth of such star-shaped NPs was already reported in the case of systems prepared by a seed mediated technique in a liquid medium or by exploiting the diffusion effect of metallic seeds deposited on a free surface [62, 63], where the confinement effect is not present. Such result leads us to conclude that the confinement effect also induce shape change as reported elsewhere.

3.2.2. Porosity Investigation

The HR-TEM micrograph (Fig. 4C) of the Co-CoO@CNT sample reveals the presence of a difference of contrast within the NP surface, which could be associated with a non-homogeneity of the chemical structure and/or morphology, whereas the HR-STEM micrographs (Fig. 4D-E) identified the presence of porosities defined as "pseudo-fractures" in the NPs structure. In order to get more insight about the NPs shape and porosity (pores

size, geometry, opening and accessibility) transmission electron tomography analyses were performed, using the incoherent STEM-HAADF acquisition mode. The results are summarized in Figure 6 and an animation of the 3D modelling is included in Supplementary Information part 6. The qualitative analysis of the reconstructed volume provides direct evidence on the 3D octahedral shape of the NPs. A careful analysis of the slices redrawn from the reconstructed volume shows the presence of several individual nanocrystals with different sizes and shapes separated by pores (see the individual modes of a NP and its schematic representation from Fig. 7 A, B). The HR HAADF-STEM image presented in Figure 7C shows their close crystallographic orientation, suggesting a supercrystal-type arrangement (Fig. S7 for a similar analysis performed on other particles). Such a type of arrangement is marked by the presence of pores with geometry defined by sharp edges oriented parallel to the crystal faces. The crystallographic orientation observed here can be interpreted as the results of the sintering of the cobalt NPs clusters during the heating process. Indeed thermolysis and solvothermal synthesis are known to favour the formation of colloidal nanoparticle clusters and the key parameter is the concentration in capping ligands which has to be not enough to protect the primary NPs against aggregation but sufficient to

stabilize the resulting 3D nanostructures [64]. In addition, the synthesis conditions in a confinement space should favour a reduce amount of ligands and thus the formation of NPs clusters. The nanostructure of octahedral NPs observed by TEM suggest a sintering of NPs clusters during the synthesis process: this was confirmed by experiments slowing the decomposition of cobalt stearate which show the formation of NPs cluster inside CNTs. Furthermore, it has been recently shown that such clustering may be favoured by magnetic interactions [65]. Indeed the diameter of cobalt NPs is very close to the superparamagnetic-ferromagnetic diameter limit and it is well-known that aggregation is a common feature of NPs synthesis and can occur as a function of the amount and type of capping agents and the magnetic effects [65]. Thus the octahedral shape NPs results from a clustering of cobalt NPs induced by both the low amount of capping ligands and magnetic interactions while the pores observed inside the NPs are resulted from an aggregation of small cobalt clusters during the growth process. According to the TEM tomography results (Fig. 7B) part of the pores are well connected from each other through the CoO-Co nanoparticles. In conclusion, solvothermal synthesis and confinement effect lead to the formation of porous Co-based nanoparticles.

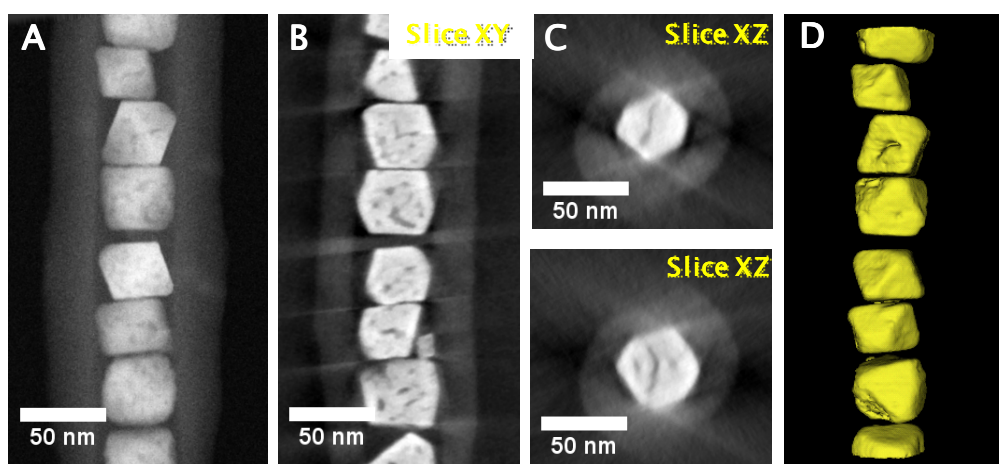


Fig. 6 (A) STEM-HAADF micrograph at 0° tilt extracted from the tilt series used to reconstruct the volume of the studied object; (B) Transversal and (C) longitudinal slices taken at different heights and orientations from the reconstructed volume. (D) 3D tomographic model of several Co-based nanoparticles with octahedral shape casted inside a CNT. The cobalt NPs are oriented in different directions with respect to the CNTs channel in order to maximize the packing.

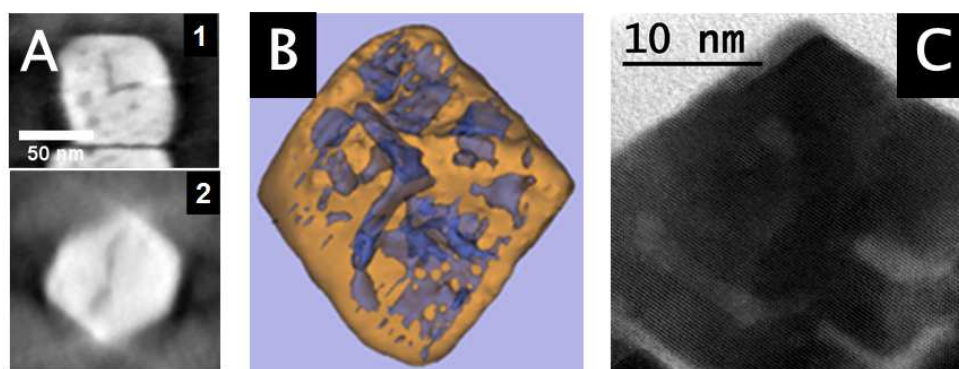


Fig. 7 (A) Two typical slices from the reconstruction calculated from the HAADF-STEM tilt series, through the sub-volume of an individual nanoparticle illustrating the presence of pseudo-fractures inside the NPs, oriented parallel to the lateral facets. (B) 3D tomographic model of the selected nanoparticle showing its octahedral shape as well as pseudo-fractures and/or voids (in blue) within the nanoparticle. (C) HR-STEM image on a typical nanoparticle allowing the observation of unique crystallographic network while the pores can be visualized as bright zones inside the particle.

Cite this: DOI: 10.1039/c0xx00000x

PAPER

www.rsc.org/xxxxxx

To investigate the porosity parameters, the samples Co/CNTs and Co/FLG were further characterized by BET technique. Table 1 summarizes the specific surface (S_{BET}), the pores volume (V_{total}) and size (D_{BJH}) of Co-based/CNTs and Co-based/FLG in comparison with the correspondent CNTs and FLG without NPs.

Table 1. Specific surface, volume and size of pores obtained from the BET of CNTs, Co-based/CNTs, FLG and Co-based/FLG samples

| Sample | S_{BET} (m ² /g) | V_{total} (cm ³ /g) | D_{BJH} (nm) |
|---------|--------------------------------------|---|-----------------------|
| CNTs | 10.2 | 0.058 | 47.1 |
| CNTs/Co | 21.6 | 0.124 | 19.1 |
| FLG | 21.4 | 0.103 | 19.3 |
| FLG/Co | 8.7 | 0.022 | 17.5 |

For the CNTs the S_{BET} was found to be higher after the introduction of NPs, which indicate the presence of new component with a high surface/volume ratio, i.e. Co NPs. The pores volume of the Co/CNTs also increase which is in good agreement with the porous structure of the metal NPs. In contrast, the Co/FLG present a lower S_{BET} compared to the pristine FLG which could be attributed to the presence of large cobalt particles with low specific surface according to the TEM analysis.

3.2.2. Magnetic properties.

The magnetic properties of the synthesized Co-based NPs encapsulated in CNTs were investigated by carrying out measurements of magnetization as a function of an applied external magnetic field at 5 K and 400 K (Fig. 8). For both temperatures, the magnetization curves display hysteresis loops (characteristic of NPs magnetically active below their blocking temperature (TB)). The saturation magnetization (M_s), at 5 K, was found to be 57 emu.g⁻¹, which is much lower than the M_s value of bulk cobalt (168 emu.g⁻¹).

Such a low magnetization is usually ascribed to defects and/or spin canting (modification of the super-exchange angles, the values of coupling and magnetic moments) within the volume and/or at the surface of the particles [66-68]. The presence of oxidized layer of antiferromagnetic CoO at the NPs surface (the presence of Co₃O₄ being excluded by the XRD analysis) also explains this relatively low magnetization value. The coercive field measured at 5 K and 400 K are about 470 Oe and 320 Oe respectively, and also related to these facts.

The magnetic behavior at the macroscopic scale was confirmed by applying an external magnet to a suspension containing the sample (Fig. inset). After 5 min of contact, the

quasi-totality of the NPS@CNTs was attracted to the surface of the vial in contact with the magnet, which is of great interest for applications in catalysis (to realize a magnetic separation of catalysts) or in the biomedical field (for driving the composite position in the physiologic or biologic mediums).

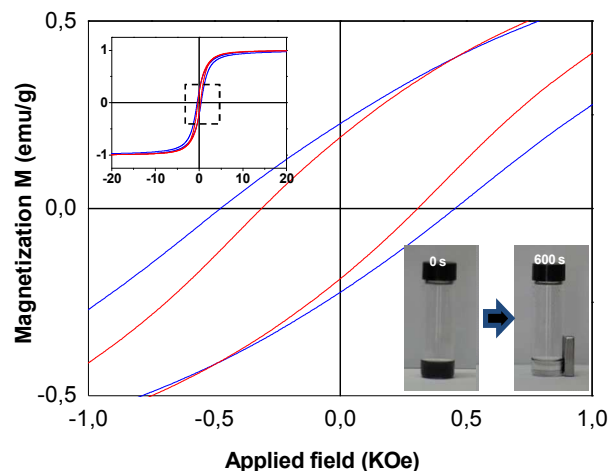


Fig. 8 Magnetization curves as a function of the applied magnetic field of Co based NPs encapsulated inside CNTs measured at 5 K (blue) and 400 K (red). Inset, top: zoom out on hysteresis loops, showing the saturation of magnetization; down: optical photos of the cobalt-based NPs@CNTs solution after ultra-sonication (0 s) and after contacting with an external magnet for 600 s.

3.3. Metallic Co@CNTs: Microstructure after reduction

According to the previous results the cobalt NPs are consisted by a metal core surrounded by a CoO shell. This part of the work is devoted to the study of the impact of the reduction process (under H₂ atmosphere at 400°C) on the microstructure of the Co-based NPs@CNTs, i.e. influence of the reduction process on the microstructure of the hybrid Co-CoO core-shell NPs. The TEM micrographs (Fig. 9) show that such a treatment not only modifies the crystalline structure of the NPs but their external shape as well. More specifically, the well-defined facets of the octahedral as-synthesized NPs have lost their sharpness and the NPs are rather constituted by pseudo-cubic aggregates of smaller entities (around 5 nm) separate by pores.

In fact, one may advance the hypothesis of NPs "explosion" due to the reduction treatment, which could be in agreement with the formation of octahedral non reduced NPs by oriented aggregation induced by the CNT confinement. As it can be deduced from Figure 8, the reduction occurs along the facets and grain boundaries of the former NPs aggregates. The pseudo-fractures being opened under the impact of the reduction process, but being confined in the CNTs channel. During the reduction process the CoO shell oxide surrounding the cobalt metal clusters is converted into cobalt metal leading to a modification in the apparent density and thus, fracturing occurs leading to the porous

NPs with several aggregates of small cobalt clusters. The observed pseudo-morphism transformation is in agreement with the Kirkendall mechanism [69], which explains the formation of the larger voids within the NP by the diffusion of chemical species along the crystallographic defects, represented here by the fractures.

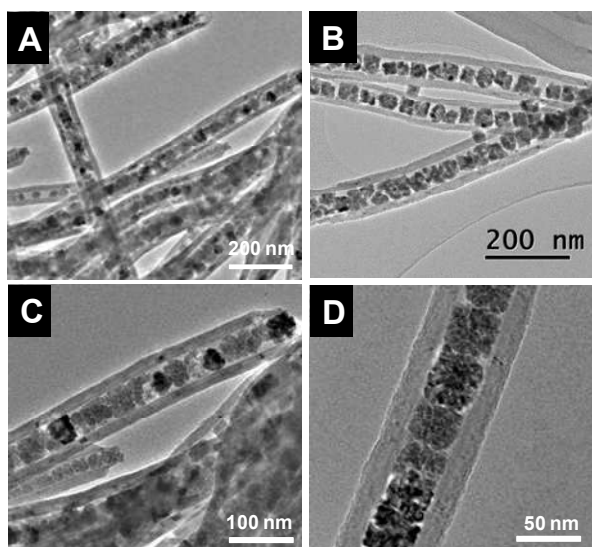


Fig. 9 Representative TEM micrographs of Co@CNTs after reduction at 400 °C for 2 hours under H₂.

Similar structural change leading to the formation of porous structure has already been reported by Pham-Huu and co-workers : during the pseudomorphism transformation of a low specific surface area MoO₃, either bulk and supported on SiC, under H₂ and C₆H₁₄ into a highly porous MoO_xC_y structure while the macroscopic shape remains almost unchanged [70-71]. The formation of a higher amount of pores inside the MoO₃ consecutively to the oxide to carbide transformation also increases the effective surface area of the small cobalt clusters for subsequent reaction.

The crystalline structure of the reduced NPs was analyzed by XRD in the range of 30–57° (Fig. 10A). The XRD pattern clearly shows the absence of CoO peaks ((111) and (200) at 37° and 42° (2θ), respectively), which were present in the initial XRD pattern of the Co-based NPs prior to reduction. The refinement of the XRD pattern also reveals the presence of both alpha and beta crystalline phases of cobalt (JCPDS files n°01-89-4307 and 01-89-4308, respectively). Indeed, the HR-TEM micrograph (Fig. 9D) shows that the density of the pseudo-fractures within the reduced NPs is considerably higher than for the as-prepared specimen, which is confirmed by the strong contrast in the HR-HAADF-STEM micrographs in Fig. 10B. This finding backs up our previous result on the NPs porous character after reduction and such porosity could be explained by the transformation of the CoO phase, principally present on the grain boundary into pure metallic cobalt. From the crystallographic point of view, cobalt, as metal, is denser than its corresponding oxide. One can therefore consider pseudo-fracture opening and subsequent differentiation of the cobalt crystals. Obviously, the sizes of the resulting pores are considerably higher than the spacing between the cracks edges within the non-reduced specimen (Fig. 10C).

According to the TEM analysis a large part of the pores and channels created inside the cobalt NPs are directly connected to the outside of the particle which significantly improve the accessibility of the clusters localized within the particle.

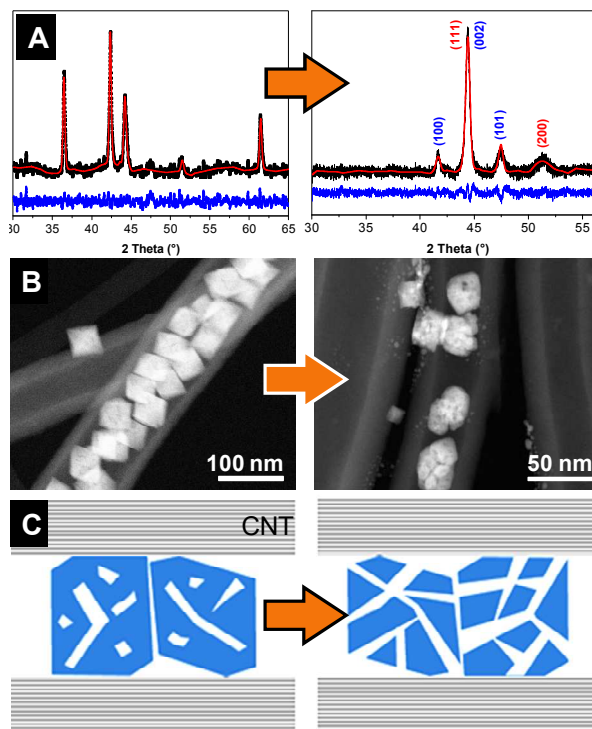


Fig. 10 (A) XRD pattern of the CNTs containing cobalt NPs prior (left side) and after reduction (right side) showing the presence of alpha-Co (red) and Beta-Co (blue) after the hydrogen assisted thermal treatment; (B) HAADF-STEM images showing the fractured character of the reduced nanoparticles casted inside the CNT channel, as compared to initial system; and (C) Schematic representation of the microstructure changes (pseudo-fractures opening) induced by the reduction leading to the formation of connected pores running through the particle.

Such porosity is of high interest as it allows the reactant to fully access to the active sites localized in the particle core and also for the escaping of the intermediate products. It is also worthy to note that the reduced sample remains in its metallic state after air exposure according to the XRD analysis, despite that some superficial oxidation cannot be evidenced by the XRD technique, and confirm again the significant role of the CNTs to prevent excessive oxidation of small metal clusters inside its channel which is not the case for unprotected small metal clusters where spontaneous oxidation occurs upon air exposure.

3.4. Dynamical morphological change of Co based@CNTs under heating by in situ TEM

In this section the morphological change and sintering behaviour as a function of the heating temperature will be investigated on both Co-CoO@CNT (after synthesis) and Co@CNT (after reduction under hydrogen at 400°C). The morphological and sintering resistance were conducted with in situ heating inside the TEM holder specimen and the change was monitored continuously.

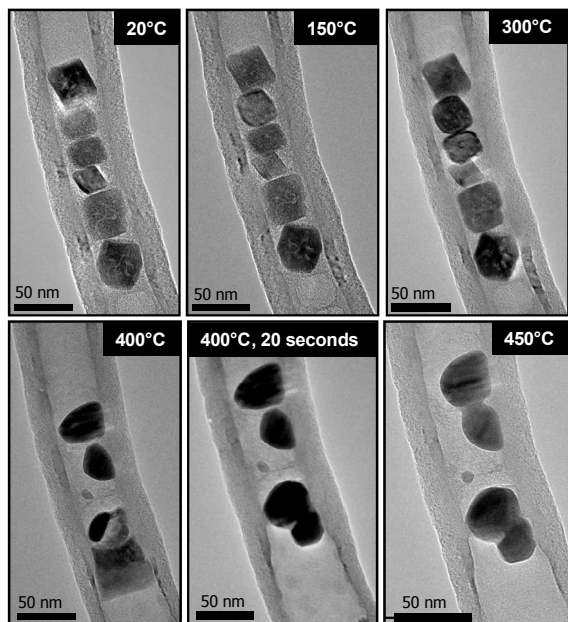


Fig. 11 *In situ* TEM analysis of Co-CoO based NPs@CNT structure through heating process under vacuum.

Fig. 11 presents the *in situ* TEM micrographs recorded at different temperatures on the same unreduced Co-CoO NPs@CNTs object. At 300 °C, the shape and internal structure of the NPs are slightly modified and becoming more compact and less faceted, the fractures, visualized as white areas inside the NPs, become less visible which indicate that the sintering process is started even at such low processing temperature. At 400 °C, the morphological modification is become more evidence and the

NPs are changed from octahedral to rounded shape with a consecutive creation of a relatively smooth cobalt-carbon interface. At 400°C the NPs also display a coalescence mechanism between neighbouring particles as shown in Fig.11. The coalescence of NPs at 400 °C, (less than the bulk phase transition [72]) can be justified by considering the relatively strong interactions between the Co-CoO NPs and the inner wall of the CNTs which leads to a rapid shape modification and sintering of the NPs upon heating at 400°C. The sharpness interface between the Co-based NP and the CNT's inner wall could be attributed to the formation of a thin layer of carbide during the heating process [73]. In such transformation part of the carbon layer was reacted with the oxygen in the CoO leading to the formation of CO₂ and carbide interface.

On the contrary the reduced Co NPs@CNTs displays a radically different sintering behaviour during the thermal treatment step (Fig. 12). No morphological change was observed upon heating at 430°C as the system has already been reduced at 400°C under H₂. At temperature of 600°C some coalescence and breaking are observed in the system which could be attributed to the thermal movements of the nanoparticles. At treatment temperature approaching 700°C shrinkage of the cobalt NPs is observed due to the pore surface diffusion leading to a denser particle. It is worth noting that in the case of pre-reduced cobalt NPs the annealing process do not lead to the formation of a homogeneous and smooth cobalt-carbon interface, i.e. carbide-like, as observed in the un-reduced sample (Fig. 12 versus Fig. 11). Such phenomenon could be attributed to the lack of reaction between the outer cobalt oxide and the carbon surface as encountered with the Co-CoO@CNTs sample and thus, it is expected that no carbide interface was generated in this case.

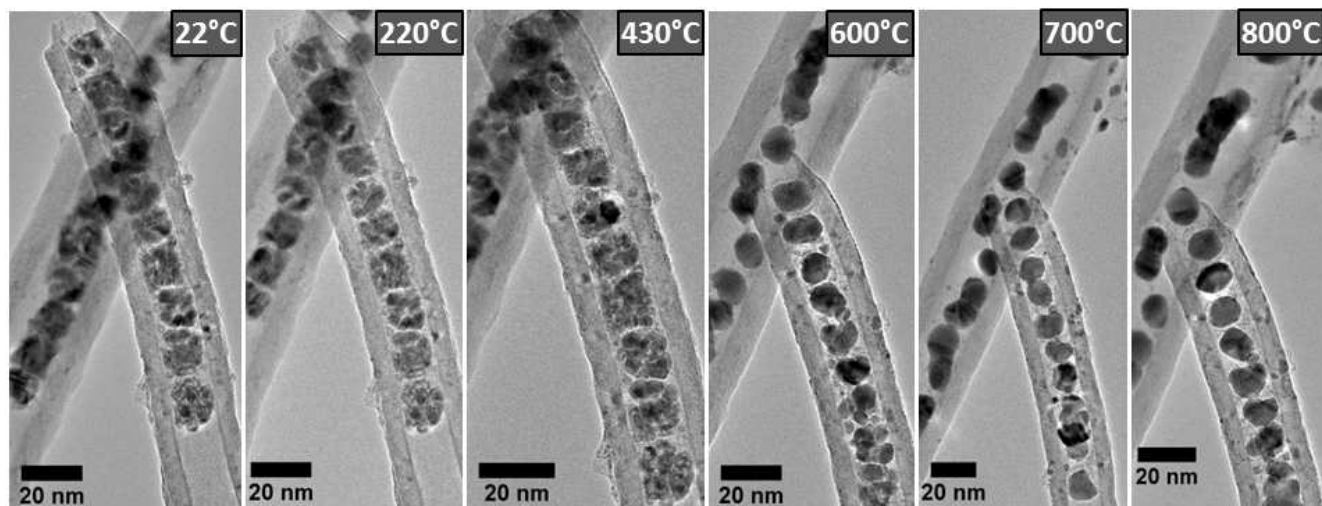


Fig. 12 Thermal evolution of metallic (reduced) Co@CNT system investigated by *in-situ* TEM experiments. The change in the NPs shape upon heating could be associated with the porosity loss of the NPs.

Even in the high temperature range (800°C) the cobalt particles with diameter around 10 nm are still observed. Such result is very striking as it is usually observed that cobalt clusters are sinter at relatively low temperature especially in this diameter range. The high resistance towards sintering of the cobalt clusters is attributed to the peculiar behaviour of cobalt metal nanoparticles in a confinement medium which provide nanoscale dimension surface for the stabilization of these metal clusters.

The main difference between the non-reduced and reduced system, in terms of their thermal behaviour, is the temperature at which the particles have lost their pseudo-porous structure and become compact. In addition, compared to the Co-CoO@CNT sample the pre-reduced one exhibit a net higher sintering resistance as the cobalt NPs remain almost separated from each other throughout the annealing step.

4. Conclusion

In summary, we have shown the role on the confinement effect within the carbon nanotubes (CNTs) channels as unique control of the structure and morphology of Co-based nanoparticles (NPs).

This effect was found to generate cobalt-like NPs with octahedral shapes and highly exposed facets and with morphologies fundamentally different from the classical round-shaped or needle-like shapes obtained in the absence of the confinement effect. The confinement effect leads to a significant improvement of the oxidative resistance of the confined cobalt NPs compared to the un-confined cobalt NPs. Such result could be attributed to the low diffusion of oxygen inside the nanoscale dimension of the channel which significantly reduces the oxygen exchange between the inner part and the outer medium. In this case, a careful examination of the reactivity between oxygen and inner wall CNTs defects on one hand, and the one between oxygen and casted metal NPs on the other hand should be conducted.

The quantitative application of electron tomography in the STEM mode allowed us to assign the octahedral morphology of NPs casted inside the channels of the CNTs. TEM tomography also allows one to map out the zig-zag orientation of the cobalt octahedral NPs with respect to the tube channel in order to maximize the packing. In addition, a porous structure marked by the presence of pseudo-fractures within the unique nanocrystalline network of NPs has been identified by a complete HR-STEM analysis and confirmed the formation of such a network by an orientated aggregation induced by the CNTs "nanoreactors" modifying the pressure and temperature conditions but also the supply of reactants.

Finally, in situ annealing process of the as-synthesized Co-CoO@CNTs and the same after reduction, Co@CNTs, indicates that the pre-reduction leads to the formation of porous cobalt aggregates with high exposed cobalt clusters, ca. 5 nm, which exhibits a significant improvement in the resistance towards sintering. Cobalt particles with size of around 10 nm are still observed in the CNTs channel after an annealing step at 800°C. It is worthy to note that such high resistance towards sintering has not been reported so far in the literature and indicate that confinement effect could be a useful method for the production of new hybrid system with enhanced physical properties compared to the traditional ones.

The peculiar physical properties of these porous metal NPs confined inside the carbon nanotubes channel, i.e. high resistance towards oxidation, high effective surface area and improved sintering behaviour, could be extremely helpful for being used as a new class of heterogeneous catalyst in harsh reaction conditions or as magnetic driven catalyst in liquid-phase reactions. Work is ongoing to evaluate the use of such sample as magnetic support for precious metal in the selective hydrogenation of unsaturated hydrocarbon compounds or directly as an active phase for the Fischer-Tropsch synthesis process where nanometer cobalt particles with high resistance towards sintering are of great interest.

Acknowledgements

The authors acknowledge Benoit P. Pichon and Alain Derory (IPCMS) for performing the magnetic separation and magnetic

measurements and helpful discussion. The TEM experiments were carried out at the facilities of the IPCMS (UMR 7504).

Electronic Supplementary Material

Supplementary material (XPS survey scan spectra of the pristine CNTs and those heated at 650°C in UHV (SI1), TGA curve of the Co-based NPs@CNTs and size distribution of Co-based NPs (SI2), TEM images of the Co-based NPs inside a CNT's channel with closed end (SI3), HAADF-STEM image and corresponding EELS spectra of CoO/ FLG (SI4), TEM image of the CoO/FLG system (SI5), Video of 3D modelling (SI6) and HR HAADF-STEM analysis of Co-based NPs inside the CNTs (SI7)) is available in the online version of this article

Notes

⁷⁰ ^a Institut de Chimie et Procédés pour l'Energie, l'Environnement et la Santé (ICPEES), ECPM, UMR 7515 du CNRS, Strasbourg University, 25 rue Becquerel, 67087 Strasbourg Cedex 02, France; Tel: +33 (0)368 852 667; Fax: +33 (0)368 852 671; E-mail: Walid.Baaziz@ipcms.u-strasbg.fr

⁷⁵ ^b Institut de Physique et Chimie des Matériaux de Strasbourg (IPCMS), UMR 7504 du CNRS, Strasbourg University, 23 rue du Loess, 67037 Strasbourg Cedex 08, France;

⁸⁰ ^c Laboratoire de Physique des Interfaces et Couches Minces, UMR 7647 CNRS-Ecole Polytechnique, Route de Saclay, 91128, Palaiseau-Cedex, France

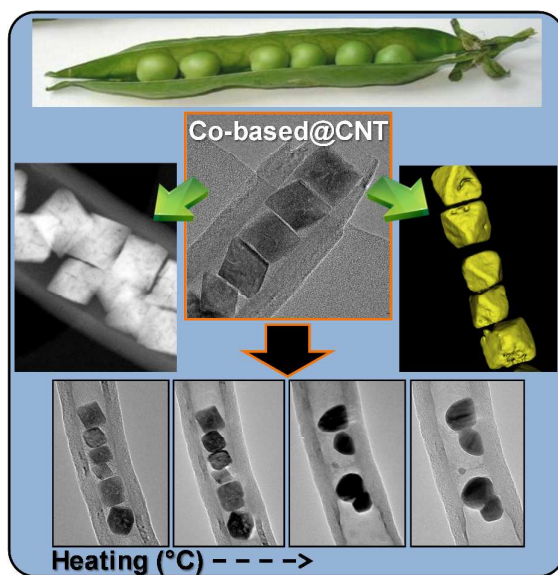
References

- 1 S. C. Tsang, V. Caps, I. Paraskevas, D. Chadwick, D. Thompsett, *Angew. Chem. Int. Ed.*, 2004, **43**, 5645–5649.
- 2 C. H. Jun, Y. J. Park, Y. R. Yeon, J. R. Choi, W. R. Lee, S. J. Ko, J. Cheon, *Chem. Commun.*, 2006, **15**, 1619–1621.
- 3 U. Laska, C. G. Frost, P. K. Plucinski, G. Price, *J. Catal. Lett.*, 2008, **122**, 68–75.
- 4 Y. Wu, T. Zhang, Z. Zheng, X. Ding, Y. Peng, *Mat. Res. Bull.*, 2010, **45**, 513–517.
- 5 K. Aranishi, H. L. Jiang, T. Akita, M. Haruta, Q. Xu, *Nano Res.*, 2011, **4**, 1233–1241.
- 6 Magnetic Nanoparticles: From Fabrication to Biomedical and Clinical Applications, Editeur Thanh Nguyen, Taylor&Francis, 2011.
- 7 J. Kim, Y. Piao, T. Hyeon, *Chem. Soc. Rev.* 2009, **38**, 372–390.
- 8 C. Fang, M. Zhang, *J. Mater. Chem.*, 2009, **19**, 6258–6266.
- 9 M. Liong, J. Lu, M. Kovichich, T. Xia, S. G. Ruehm, A. E. Nel, F. Tamanoi, J. I. Zink, *ACS Nano.*, 2008, **2**, 889–896.
- 10 M. De, P. S. Ghosh, V. M. Rotello, *Adv. Mater.*, 2008, **20**, 4225–4241.
- 11 A. K. Gupta, M. Gupta, *Biomaterials.*, 2005, **26**, 3995–4021.
- 12 L. H. Reddy, J. L. Arias, J. Nicolas, P. Couvreur, *Chem. Rev.*, 2012, **112**, 5818–5878.
- 13 S. Minocha, R. J. Mumper, *Small.*, 2012, **8**, 3289–3299.
- 14 Y. Xu, M. Mahmood, Z. Li, E. Dervishi, S. Trigwell, V. P. Zharov, N. Ali, V. Saini, A. R. Biris, D. Lupu, D. Boldor, A. S. Biris, *Nanotechnology.*, 2008, **19**, 435102–435108.
- 15 P. Y. Keng, B. Y. Kim, I. B. Shim, R. Sahoo, P. E. Veneman, N. R. Armstrong, H. Yoo, J. E. Pemberton, M. M. Bull, J. J. Griebel, E. L. Ratcliff, K. G. Nebesny, J. Pyun, *ACS nano.*, 2009, **3**, 3143–3157.
- 16 Y. Liang, H. Wang, J. Zhou, Y. Li, J. Wang, T. Regier, H. Dai, *J. Am. Chem. Soc.*, 2012, **134**, 3517–3523.
- 17 S. Iijima, *Nature*, 1991, **354**, 56–58.
- 18 S. C. Tsang, Y. K. Chen, P. J. F. Harris, M. L. H. Green, *Nature.*, 1994, **372**, 159–162.
- 19 B. C. Satishkumar, A. Govindaraj, J. Mofokeng, G. N. Subbanna, C. N. R. Rao, *J. Phys. B: At. Mol. Opt. Phys.*, 1996, **29**, 4925–4934.

- 20 E. J. García, A. J. Hart, B. L. Wardle, A. H. Slocum, *Nanotechnology*, 2007, **18**, 165602.
- 21 E. Fidiani, P. M. F. J. Costa, A. U. B. Wolter, D. Maier, B. Buechner, S. Hampel, *J. Phys. Chem. C*, 2013, **117**, 16725–16733.
- 5 22 D. Ugarte, A. Châtelain, W. A. de Heer, *Science*, 1996, **274**, 1897–1899.
- 23 D. A. Britz, A. N. Khlobystov, K. Porfyrakis, A. Ardavan, G. A. D. Briggs, *Chem. Commun.*, 2005, **1**, 37–39.
- 10 24 J. P. Tessonnier, G. Winé, C. Estournès, C. Leuvre, M. J. Ledoux, C. Pham-Huu, *Catalysis Today*, 2005, **102-103**, 29–33.
- 25 O. Ersen, S. Bégin, M. Houllé, J. Amadou, I. Janowska, J. M. Grenèche, C. Crucifix, C. Pham-Huu, *Nano Lett.*, 2008, **8**, 1033–1040.
- 15 26 Y. Yao, G. S. Chaubey, J. B. Wiley, *J. Am. Chem. Soc.*, 2012, **134**, 2450–2452.
- 27 E. Castillejos, P. J. Deboutière, L. Roiban, A. Solhy, V. Martinez, Y. Kihn, O. Ersen, K. Philippot, B. Chaudret, P. Serp, *Angew. Chem., Int. Ed.*, 2009, **48**, 2529–2533.
- 28 Y. Wang, H. J. Zhang, L. Lu, L. P. Stubbs, C. C. Wong, J. Lin, *ACS Nano*, 2010, **4**, 4753–4761.
- 20 29 X. Xie, Y. Li, Z. Q. Liu, M. Haruta, W. Shen, *Nature*, 2009, **458**, 746–749.
- 30 Y. Liu, I. Florea, O. Ersen, C. Pham-Huu, C. Meny, *Chem. Commun.*, 2015, **51**, 145–148.
- 25 31 Z. Tang, N. Kotov, *Adv. Materials*, 2005, **17**, 951–962.
- 32 H. Wu, R. Zhang, X. Liu, D. Lin, W. Pan, *Chem. Mater.*, 2007, **19**, 3506–3511.
- 33 S. Srivastava, N. A. Kotov, *Soft Matter*, 2009, **5**, 1146–1156.
- 34 Y. Lalatonne, J. Richardi, M. P. Pileni, *Nat. Mater.*, 2004, **3**, 121–125.
- 30 35 S. Pal, S. Chandra, M. H. Phan, P. Mukherjee, H. Srikanth, *Nanotechnology*, 2009, **20**, 485604–485610.
- 36 W. Baaziz, X. Liu, I. Florea, S. Bégin-Colin, B. P. Pichon, C. Ulhaq, O. Ersen, M. Soria-Sánchez, S. Zafeiratos, I. Janowska, D. Bégin, C. Pham-Huu, *J. Mater. Chem. A*, 2013, **1**, 13853–13861.
- 35 37 L. Fu, Z. Liu, Y. Liu, B. Han, P. Hu, L. Cao, D. Zhu, *Adv. Materials*, 2005, **17**, 217–221.
- 38 M. Trepanier, A. Tavasoli, A. K. Dalai, N. Abatzoglou, *App. Cat. A: General*, 2009, **353**, 193–202.
- 39 X. Wang, N. Li, L. D. Pfefferle, G. L. Haller, *Microporous and Mesoporous Materials*, 2013, **176**, 139–144.
- 40 40 P. M. F. J. Costa, J. Sloan, T. Rutherford, M. L. H. Green, *Chem. Mater.*, 2005, **17**, 6579–6582.
- 41 Q. H. Do, J. Smithyman, C. Zeng, C. Zhang, R. Liang, J. P. Zheng, *Journal of Power Sources*, 2014, **248**, 1241–1247.
- 45 42 I. M. Fabiani, M.-C. G. Gutiérrez, D. R. Rueda, A. Linares, J. J. Hernández, T. A. Ezquerro, M. Reynolds, *ACS Appl. Mater. Interfaces*, 2013, **5**, 5324–5329.
- 43 W. Baaziz, S. Bégin-Colin, B. P. Pichon, I. Florea, O. Ersen, S. Zafeiratos, R. Barbosa, D. Bégin, C. Pham-Huu, *Chem. Mater.*, 2012, **24**, 1549–1551.
- 50 44 I. Janowska, T. Romero, P. Bernhardt, F. Vigneron, D. Bégin, O. Ersen, M. J. Ledoux, C. Pham-Huu, *Carbon*, 2012, **50**, 3092–3116.
- 45 45 D. N. Mastrorade, *Journal of Structural Biology*, 1997, **120**, 343–352.
- 55 46 R. Gordon, R. Bender, G. T. Herman, *J. Theor. Biol.*, 1970, **29**, 471–481.
- 47 C. Messaoudii, T. Boudier, C. O. S. Sorzano, S. Marco, *BMC Bioinformatics*, 2007, **8**, 288–297.
- 48 <http://u759.curie.u-psud.fr/software/u759.html>.
- 60 49 <http://www.Slicer3D.org>.
- 50 J. Rodríguez-Carvajal, *Physica. B*, 1993, **192**, 55–69.
- 51 P. Thompson, D. E. Cox, J. B. Hastings, *J. Appl. Cryst.*, 1987, **20**, 79–83.
- 52 O. Ersen, J. Werckmann, M. Houllé, M. J. Ledoux, C. Pham-Huu, *Nano Lett.*, 2007, **7**, 1898–1907.
- 65 53 J. Prasek, J. Drbohlavova, J. Chomoucka, J. Hubalek, O. Jasek, V. Adam, R. Kizek, *J. Mater. Chem.*, 2011, **21**, 15872–15884.
- 54 M. Kumar, Y. Ando, *J. Nanosci. Nanotechnol.*, 2010, **10**, 3739–3758.
- 55 Y. Li, W. Zhou, H. Wang, L. Xie, Y. Liang, F. Wei, J. C. Idrobo, S. J. Pennycook, H. Dai, *Nat. Nanotechnol.*, 2012, **7**, 394–400.
- 70 56 S. A. C. Carabineiro, M. F. R. Pereira, J. N. Pereira, C. Caparros, V. Sencadas, S. Lanceros-Mendez, *Nanoscale Res. Lett.*, 2011, **6**, 302.
- 57 W. Baaziz, P. B. Pichon, S. Fleutot, Y. Liu, C. Lefevre, J. M. Grenèche, M. Toumi, T. Mhiri, S. Bégin-Colin, *J. Phys. Chem. C*, 2014, **118**, 3795–3810.
- 75 58 A. Demortière, P. Panissod, B. Pichon, G. Pourroy, D. Guillon, B. Donnio, S. Bégin-Colin, *Nanoscale*, 2011, **3**, 225–232.
- 59 V. Georgakilas, D. Gourmis, V. Tzitzios, L. Pasquato, D. M. Guldi, M. Prato, *J. Mater. Chem.*, 2007, **17**, 2679–2694.
- 80 60 X. Pan, X. Bao, *Chem. Commun.*, 2008, 6271–6281.
- 61 J. M. Nhut, P. Nguyen, C. Pham-Huu, N. Keller, M. J. Ledoux, *Catal. Today*, 2004, **91**, 91–97.
- 62 L. M. Bronstein, J. E. Atkinson, A. G. Malyutin, F. Kidwai, B. D. Stein, D. G. Morgan, J. M. Perry, J. A. Karty, *Langmuir*, 2011, **27**, 3044–3050.
- 85 63 H. You, S. Yang, B. Ding, H. Yang, *Chem. Soc. Rev.*, 2013, **42**, 2880–2904.
- 64 Z. Lu, Y. Yin, *Chem. Soc. Rev.*, 2012, **41**, 6874–6887.
- 65 A. P. LaGrow, B. Ingham, M. F. Toney, R. D. Tilley, *J. Phys. Chem. C*, 2013, **117**, 16709–16718.
- 90 66 T. J. Daou, J. M. Grenèche, G. Pourroy, S. Buathong, A. Derory, C. Ulhaq-Bouillet, B. Donnio, D. Guillon, S. Bégin-Colin, *Chem. Mater.*, 2008, **20**, 5869–5875.
- 67 M. P. Morales, S. Veintemillas-Verdaguer, M. I. Montero, C. J. Serna, A. Roig, L. Casas, B. Martínez, F. Sandiumenge, *Chem. Mater.*, 1999, **11**, 3058–3064.
- 95 68 J. F. Dayen, V. Faramarzi, M. Pauly, N. T.; Kemp, M. Barbero, B. P. Pichon, H. Majjad, S. Bégin-Colin, B. Doudin, *Nanotechnology*, 2010, **21**, 335303–335310.
- 100 69 A. D. Smigelskas, E. O. Kirkendall, *Trans. AIME*, 1947, **171**, 130–142.
- 70 P. Delporte, C. Pham-Huu, M. J. Ledoux, *Appl. Catal. A: Gen.*, 1997, **149**, 151–180.
- 71 C. Pham-Huu, E. Peschiera, P. Del Gallo, M. J. Ledoux, *Appl. Catal. A: Gen.*, 1995, **132**, 77–97.
- 105 72 R. N. Grass, M. Dietiker, C. Solenthaler, R. Spolenak, W. J. Stark, *Nanotechnology*, 2007, **18**, 035703–035709.
- 73 F. J. Derbyshire, A. E. B. Presland, D. L. Trimm, *Carbon*, 1975, **13**, 111–113.
- 110
- 120

Microscopy investigations of the microstructure change and thermal response of the cobalt-based nanoparticles confined inside carbon nanotubes medium

Walid Baaziz,^{*a} Ileana Florea,^{b,c} Simona Moldovan,^b Vasiliki Papaefthimiou,^a Spiridon Zafeiratos,^a Sylvie Begin-Colin,^b Dominique Begin,^a Ovidiu Ersen,^{*b} and Cuong Pham-Huu^a



The confinement effect has been investigated on the shape, microstructure and thermal response upon heating treatment of Co-based NPs synthesized inside CNTs.